JOTCS A
Journal of the Turkish Chemical Society
Section: A
Chemistry
TURKISH CHEMICAL SOCIETY

# Molecular Dynamics Simulation of E412 Catalytic Residue Mutation of GOx-IPBCC

**Asrul Fanani[1], Popi Asri Kurniatin[1], Setyanto Tri Wahyudi[2,3], Waras Nurcholis[1,3], and Laksmi Ambarsari[1*]**

[1]Department of Biochemistry, Faculty Mathematics and Natural Sciences, IPB University, Bogor, West Java, Indonesia.
[2]Department of Physics, Faculty Mathematics and Natural Sciences, IPB University, Bogor, West Java, Indonesia.
[3]Tropical Biopharmaca Research Center, IPB University, Bogor, West Java, Indonesia.

**Abstract**: The enzyme glucose oxidase from *Aspergillus niger* has a homodimeric structure, consisting of two identical subunits with a molecular weight of 150,000 Daltons. In this study, we used the structure of the enzyme glucose oxidase from *Aspergillus niger* IPBCC.08.610 (GOx-IPBCC), this enzyme had a total activity of 92.87 U (µmol/min) and a Michaelis-Menten constant (*Km*) of 2.9 mM (millimolar). This study was conducted to predict the molecular dynamics of E412 (Glu412) residue catalytic mutation belonging to the GOx-IPBCC enzyme was determine the effect of changes in the catalytic residue on substrate binding (β-D-glucose). The results of molecular docking of 19 mutant structures, six E412 mutant homologous structures were selected (E412C, E412K, E412Q, E412T, E412, E412V, and E412W), which were evaluated using molecular dynamics simulation for 50 ns. The results showed a decrease in *ΔG* values in two mutant structures is E412C and E412T, and there is one mutant structure that increased *ΔG* values, namely E412W, these three mutant structures showed the best stability, bond interaction, and salt bridge profile according to molecular dynamics simulation.

**Keywords:** GOx-IPBCC enzyme, molecular docking, molecular dynamics simulation.

**Submitted:** March 16, 2022. **Accepted:** September 17, 2022.

**Cite this:** Fanani A, Kurniatin P, Wahyudi S, Nurcholis W, Ambarsari L. Molecular Dynamics Simulation of E412 Catalytic Residue Mutation of GOx-IPBCC. JOTCSA. 2022;9(4):1091–106.

**DOI:** https://doi.org/10.18596/jotcsa.1088587.

***Corresponding author. E-mail:** laksmi@apps.ipb.ac.id.

## INTRODUCTION

Glucose oxidase (GOx) is an enzyme that catalyzes the oxidation of β-D-glucose to gluconic acid. This enzyme works to convert glucose into gluconic acid and hydrogen peroxide with the help of oxygen (1). GOx is used industrially both to maintain glucose and to remove oxygen. An exciting application is also a unique test reagent for glucose (2). This enzyme was mainly isolated from *Aspergillus niger* (3) and *Penicillium sp* (4). GOx from Aspergillus niger has a homodimeric structure, consisting of two identical subunits with a molecular weight of 150,000 Daltons. Each subunit molecule is tightly bound to the coenzyme flavin adenine dinucleotide (FAD), which acts as a redox carrier in its catalytic reaction (5).

Until now, GOx enzymes have been widely applied in the pharmaceutical (6), chemical, and food industries, including gluconic acid production, food preservatives, and the development of biofuel cells (7). The glucose oxidase enzyme is the most widely used in daily and continuous blood glucose sensor materials (8). Glucose oxidase can also be applied in biofuel cells or self-power sensors because glucose oxidase has high specificity for glucose, low redox potential (~-0.42 V vs. Ag/AgCl at pH 7.4), and good thermostability (9,10).

In this study, we used the GOx enzyme structure of *Aspergillus niger* IPBCC.08.610 (GOx-IPBCC). This enzyme has a total activity of 92.87 U and a Km value of 2.9 mM (11,12). The 3-dimensional structure of the GOx-IPBCC enzyme was successfully predicted from the sequence of its constituent genetic code (https://www.ncbi.nlm.nih.gov/ with access number MH593586.1) (13,14). This study was conducted to predict the molecular dynamics of E412 residue catalytic mutation belonging to the GOx-IPBCC enzyme. Mutations in catalytic residues are used to determine the extent of changes in substrate binding efficiency from the dynamics of mutation changes carried out on catalytic residues, so it is hoped that this research can help the development of science related to modification of the GOx enzyme structure. The analyzes used to support the results of this study are molecular dynamics simulation (MD) and molecular mechanics Poisson Boltzmann (MMPBSA) to determine the stability of the mutant structure and to determine the bond free energy ($\Delta G$) (15,16). Until now, there have been many computational-based studies (bioinformatics) to predict the improvement of enzyme structures that can increase the stability and work of enzymes (17–19).

## EXPERIMENTAL SECTION

### *Molecular Docking Simulation*

Molecular docking simulation in this study was performed using Autodock Vina 1.1.2, with free energy (kcal/mol) value calculation parameters. 3-dimensional structure files of GOx-IPBCC enzymes and ligands were prepared using the AutoDockTools 1.5.6 tool and saved in *pdbqt format (GOx.pdbqt and ligand.pdbqt). The coordinates of the ligand-binding region (Grid box) were determined using the help of the AutoDockTools 1.5.6 tool. Furthermore, to analyze the bonding interactions (*Å*) between GOx-IPBCC and the molecular docking ligands, the Ligplot+ 1.4.5 was used to analyze results in 2D format (hydrophobic interactions and hydrogen bonds with long bond distances).

### Structural Mutation of GOx-IPBCC Enzyme

In this study, the structure of the GOx-IPBCC enzyme was mutated in the E412 catalytic region with 19 mutations. Mutations were performed using the Chimera 1.14 software following the computational mutation. The energy minimization of the mutants structures was carried out to obtain a 3-dimensional conformation in the normal state (20).

**Table 1:** The type of E412 residue mutation (glu412) of the GOx-IPBCC enzyme.

| Mutant | Mutant | Mutant |
|---|---|---|
| E412A (Ala) | E412K (Lys) | E412R (Arg) |
| E412C (Cys) | E412L (Leu) | E412S (Ser) |
| E412D (Asp) | E412M (Met) | E412T (Thr) |
| E412F (Phe) | E412N (Asn) | E412V (Val) |
| E412G (Gly) | E412P (Pro) | E412W (Trp) |
| E412H (His) | E412Q (Gln) | E412Y (Tyr) |
| E412I (Ile) | | |

### Molecular Dynamics (MD) Simulation

Molecular dynamics simulations were run using the Amber 18 (21). The ligand and protein complexes were prepared from the best models, removing unnecessary hydrogen atoms and other molecules. Next, a new hydrogen atom is added, and the protonated state of the side chain can be titrated using the Virginia Tech H++ server (http://biophysics.cs.vt.edu/H++) (22,23). After that, energy minimization was carried out for six repetitions. In the end, the system was heated gradually from 0-300 K. After the desired temperature was reached, six equilibrium steps were carried out to ensure the stability of the time-related structural properties in the initial equilibration. The first step of limiting was applied in fixed volume (NVT) for 50 ps and the subsequent phase under constant pressure (NPT). The restriction is then slowly removed for 300 ps in total. This allows the system to get the proper density and also to avoid aggregation. The final step of the simulation is a lengthy production process in which the dissolved protein is run for 50 ns of simulation in 25 separate stages of 2.0 ns each (2.0 fs timestep).

The free energy of ligand binding by proteins was calculated using the MMPBSA approach (kcal/mol) (24). The free energy is calculated using a single pass procedure, agreeing with the results obtained from molecular dynamics simulations, operating with high structural stability. This approach uses the potential energy of molecular dynamics (VDW + EEL) and the free energy of the solvent (nonpolar + polar) (16).

## RESULTS AND DISCUSSION

### Molecular Docking Validation

The 3-dimensional structure of the GOx-IPBCC enzyme did not contain ligand structure that bind to its binding site. To compare and validate the binding site, the 3-dimensional structure of the GOx-IPBCC enzyme and the 3-dimensional structure of the GOx 1CF3 enzyme with known binding site was aligned (25). On the other hand, the use of the 1CF3 structure is based on the position of this structure as the template structure for the GOx-IPBCC builder (13).

Based on the analysis results, it was found that the anchorage area was suitable and had the best results from the alignment of the GOx-IPBCC and 1CF3 structures with binding energy values of 6.0 kcal/mol and 6.6 kcal/mol. Moreover, the results of redocking with 10 repetitions obtained a binding RMSD value of 0.7.

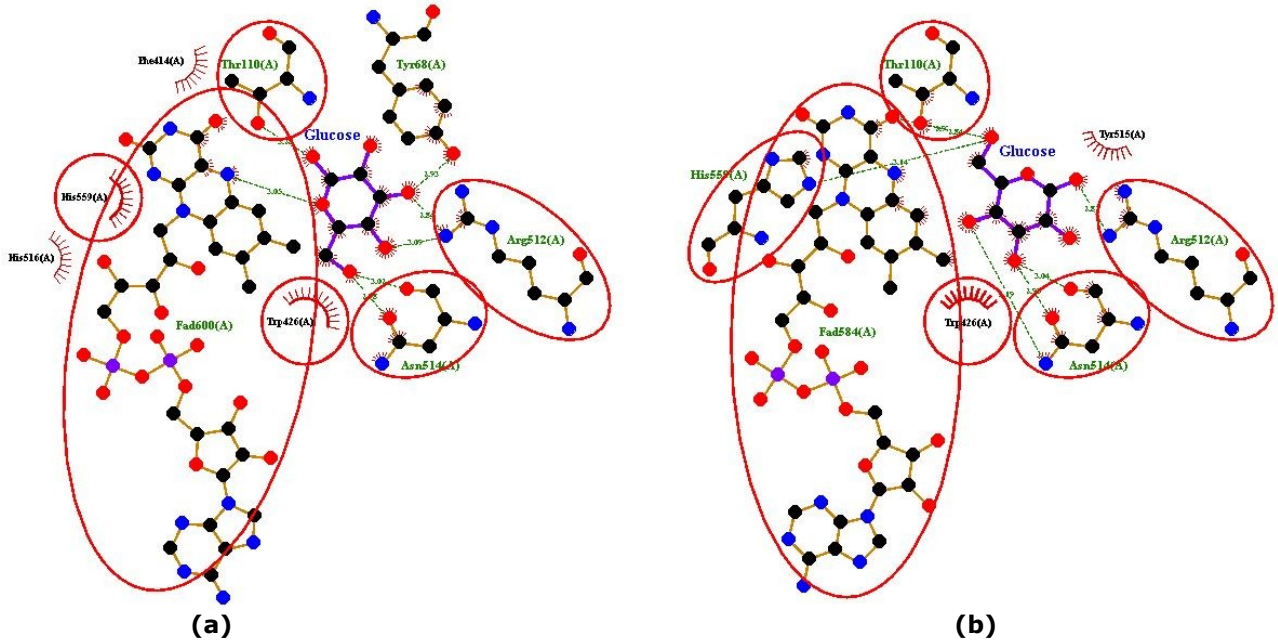


**Figure 1:** Comparison of visualization of β-D-glucose ligand binding interaction by the structures of **(a)** 1CF3 and **(b)** GOx-IPBCC.

### Structural Mutations of GOx-IPBCC Enzyme

The study of mutagenesis has a broad impact on the development of science in enzymes (26). Mu et al., (2019) reported that the mutation of the GOx enzyme structure could increase the stability of the enzyme up to a temperature of 70℃ and a pH of 4.5-7.0 and was able to convert 98% of glucose into gluconic acid. In this study, the structure of the GOx-IPBCC enzyme was single-mutated at the catalytic residue E412. There are 19 mutant structures in all (Table 1). The parameter used to compare the quality of the mutant structure are the value of *ΔG* and residue binding interactions with ligands. Based on the data obtained from the molecular docking simulation on the mutant structure, the mutation of the E412 residue in the GOx-IPBCC structure affects the binding energy of the ligand. Table 2 shows the changes in the value of *ΔG* that occur in each mutant structure.

**Table 2:** Comparative data from molecular docking simulation analysis on residue E412.

| Mutant | *ΔG* (kcal/mol) | Hydrogen bond | Hydrophobic bond |
|---|---|---|---|
| *Wild-type* | −6.0 | | |
| E412A | −6.0 | | |
| E412C | −5.9 | | |
| E412D | −5.9 | Thr110, Arg512, Asn514, His559, FAD | Trp426, Tyr515 |
| E412H | −5.9 | | |
| E412K | −6.0 | | |
| E412M | −5.9 | | |
| E412N | −6.0 | | |
| E412P | −5.7 | Thr110, Arg512, Asn514, His559, Asp424 FAD | Trp426 |

| | | | |
|---|---|---|---|
| E412S<br>E412V<br>E412W | −5.9<br>−5.7<br>−6.1 | Thr110, Arg512, Asn514, His559, FAD | Trp426, Tyr515 |
| E412F | −5.5 | Thr110, Arg512, Asn514, FAD | Trp426, Tyr515, His559 |
| E412G | −5.9 | Thr110, Arg512, Asn514, FAD | Trp426, His559 |
| E412I<br>E412L<br>E412Q | −5.7<br>−5.7<br>−5.9 | Thr110, Arg512, Asn514, FAD | Trp426, Tyr515, His559 |
| E412R | −6.0 | Arg512, Asn514, His559, FAD | Thr110, Trp426 |
| E412T<br>E412Y | −5.8<br>−5.7 | Thr110, Arg512, Asn514, FAD | Trp426, His559 |

Based on the profile of the *ΔG* values of 19 mutant structures, explicated that the mutation of the E412 residue had a significant effect on the binding energy of the receptor (GOx-IPBCC). Furthermore, were selected six mutant structures for further molecular dynamics analysis. This analysis serves to obtain further data regarding the characteristics of the mutant structure at the molecular level and its stability. The mutant structures selected were E412C, E412K, E412Q, E412T, E412V, and E412W. These six selected structures are based on the *ΔG* value and the best ligand-binding mode that is close to the wild-type structure.

**Molecular Dynamics Simulation**

Molecular dynamics is simulated to obtain molecular data statistically and dynamically to validate the data of a structure (27). The molecular dynamics simulation of the GOx-IPBCC mutant enzyme was run for 50 ns at 300 K. The RMSD data obtained in the molecular dynamics simulation describe the structure of the E412C, E412K, E412Q, E412T, E412V, and E412W mutants. That have RMSD values that are not much different from the wild type (WT) structure (Figure 2); these results confirm that the mutant structure has good structural stability, as does not have an RMSD value that is much different from the WT structure.

The following simulation data obtained is the RMSF plot. These data describe fluctuations in electron movement that occur at the level of residues (amino acids) of the GOx-IPBCC structure having high fluctuations in the N terminal and C terminal residues. However, this increase in fluctuation does not affect the stability level of the GOx-IPBCC structure. In addition, there are high enough fluctuations that also occur in the sequence residues 269-272, 255, and 259 (Figure 3). Based on the comparison data of the RMSF plot of the GOx-IPBCC mutant structure with the wild-type structure, there were quite clear differences in the fluctuations in the sequence of residues 61-73. The mutant structure experienced an increase in fluctuations in the RMSF plot of residue area 61-73. This increase occurred significantly in the E412K, E412Q, E412V, and E412W mutant structures, while in the E412C and E412T mutants, the increase was not significant (Figure 3).

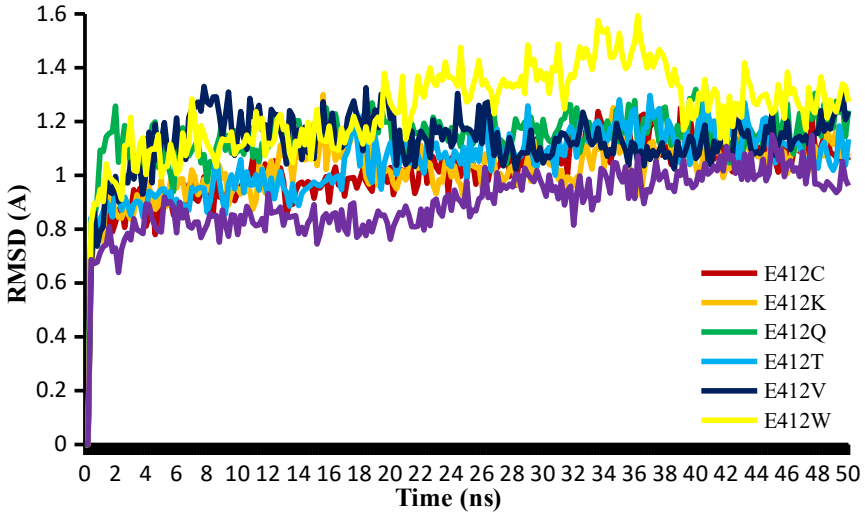


**Figure 2:** Comparative profile of the RMSD value of the GOx-IPBCC enzyme mutant structure from the 50 ns molecular dynamics simulation.

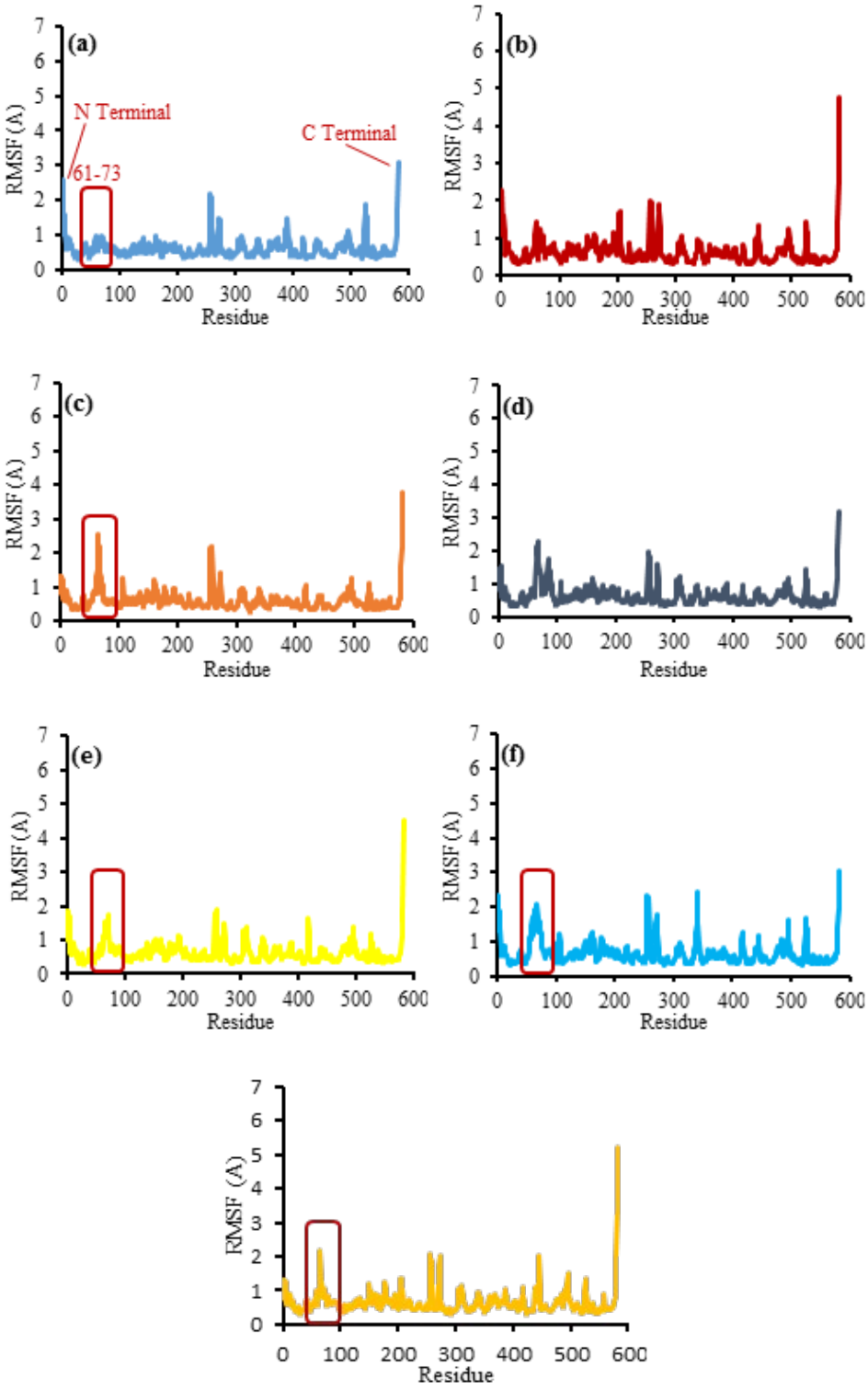


**Figure 3:** RMSF profile of GOx-IPBCC mutant during 50 ns molecular dynamics simulation at residue E412 (a) WT (b) E412C (c) E412K (d) E412Q (e) E412T (f) E412V (g) E412W.

The increase in fluctuations indicates that the level of flexibility of the residue structure increases, and residues that have low fluctuations are stiffer and, therefore, more stable (28). High fluctuations can affect the stability of the structure. The dynamics of fluctuations in the structure of the GOx-IPBCC mutant illustrate the effect of changes in the structure of one amino acid residue that can affect fluctuations in other amino acid residues. The fluctuation changes that occur are not significant, and it is difficult to determine whether the enzyme structure's stability well maintained. Thus,

secondary structure analysis needs to be carried out to determine the effect of increasing fluctuations on the secondary structure profile of the GOx-IPBCC enzyme.

**Profile of GOx-IPBCC. Mutant Secondary Structure**

Based on the analysis results obtained from the RMSF plot data, there are differences in fluctuations between the mutant and wild-type structures. This difference occurs mainly in the increasing sequence region of the residue from 61 to 73. The analysis results revealed that the residue sequence region 61-73 formed a secondary structure conformation of 3-10 helices. The 3-10 helix conformation has three rotating residues, with an angle of 120° between successive residues, the helix increment per residue 1.93–2.0. Simply put, the 3-10 helices have a tighter, longer, and thinner coil than the -helices, with the same number of residues (29).

In the wild-type structure, this conformation was maintained until the end of the simulation time (50 ns) (Figure 4). The secondary structure of the E412C and E412V mutants shows that the two mutant structures do not undergo a 3-10 helix conformational change in the residue region 61-73. The mutant structures E412K, E412Q, E412T, and E412W gave different results (Figure 5), namely that these mutant structures have 3-10 helix conformational changes during the simulation time. Mutant E412K underwent a 3-10 helix conformational change when the simulation entered 23 ns, and at 43 ns, the 3-10 helix conformation reappeared. In the E412Q, E412T and E412W mutants, there was a 3-10 helix conformational change from the beginning of the simulation time to the end of the simulation time.

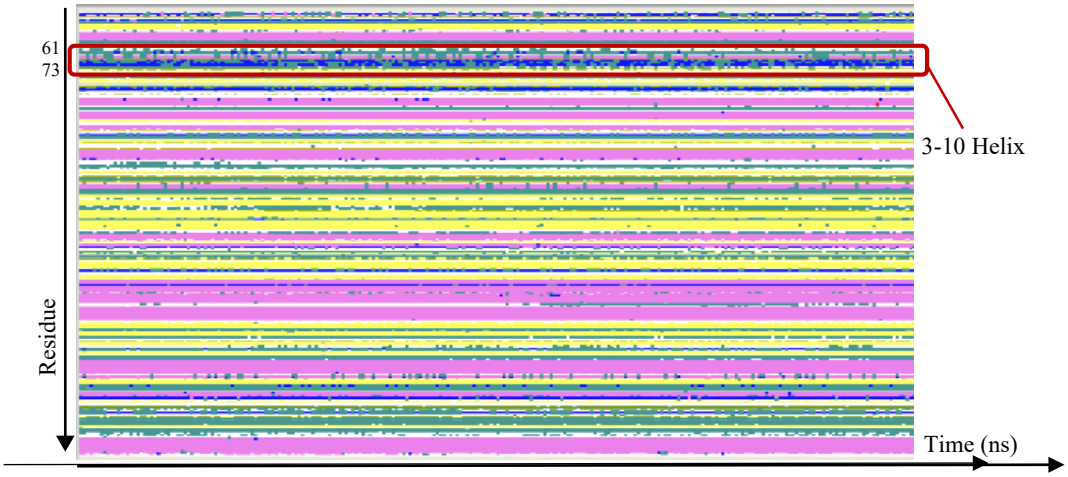


**Figure 4:** The results of analysis secondary structure enzyme GOD_IPBCC_1CF3 (wild type) during the molecular dynamics simulation time of 50 ns. *turn,* *isolated bridge,* α-helix, 3-10 helix, Pi-helix, *Extended configuration,* *coil.*

The 3-dimensional visualization was intended to determine the proximity of the 3-10 helix conformation to the mutant residue 412 (m412) and determine the effect of mutations on the interactions between amino acids in the 3D structure of the GOD-IPBCC mutant and to compare its interaction structure with the wild-type conformation (Figure 6). Based on the observations, it is obtained an image of the close interaction between the residues of the 3-10 helix conformation and the residues of mE412 in the wild type structure, which is not too far apart, and the residues of the 3-10 helix conformation are also close to the FAD cofactor.

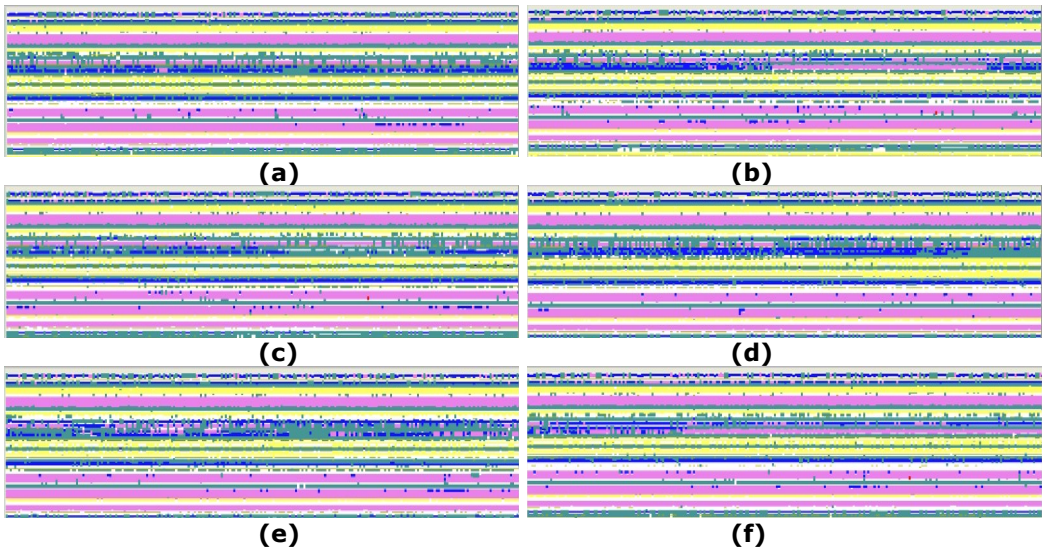


**Figure 5:** Visualization of the results of secondary structure analysis of 3-10 helix mutant residue E412 enzyme GOD_IPBCC_1CF3. (a) E412C, (b) E412K, (c) E412Q, (d) E412T, (e) E412V, (f) E412W.

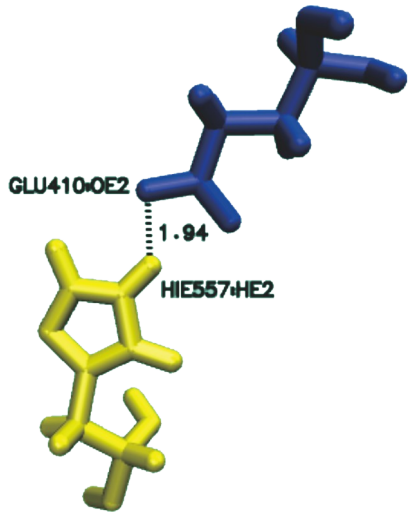


**Figure 6:** Visualization of the interaction between E412 and H559 mutant residues in the structures wild-type GOx-IPBCC.

From the observations on the structure of the GOD-IPBCC mutant, shown that what affects the stability of the 3-10 helix conformation is the proximity to residues H559 and m412. When the bond distance between residues m412 and H559 is stretched, the residue H559 tends to be unstable and closer to the 3-10 helix conformational region. Thus, the 3-10 helix conformation becomes unstable as it is disturbed by the activity of the closer H559 residue. This occurred in the E412T mutant (Figure 7d) because the bond distance between H559 and m412 became 6.61.

In contrast to what happened to the E412K, E412Q, and E412W mutants (Figure 7b, 7c, 7f). The three mutant structures had close interaction distances between H559 and m412 residues, which were 3.15, 2.95 and 2.02, respectively. However, the 3-10 helix structure was unstable. This is because the interaction of the H559-m412 residue tends to be closer to the 3-10 helix conformation when compared to the wild-type structure. This is caused by a change in the -R group of the m412 amino acid, which results in a shift closer to the 3-10 helix conformation.

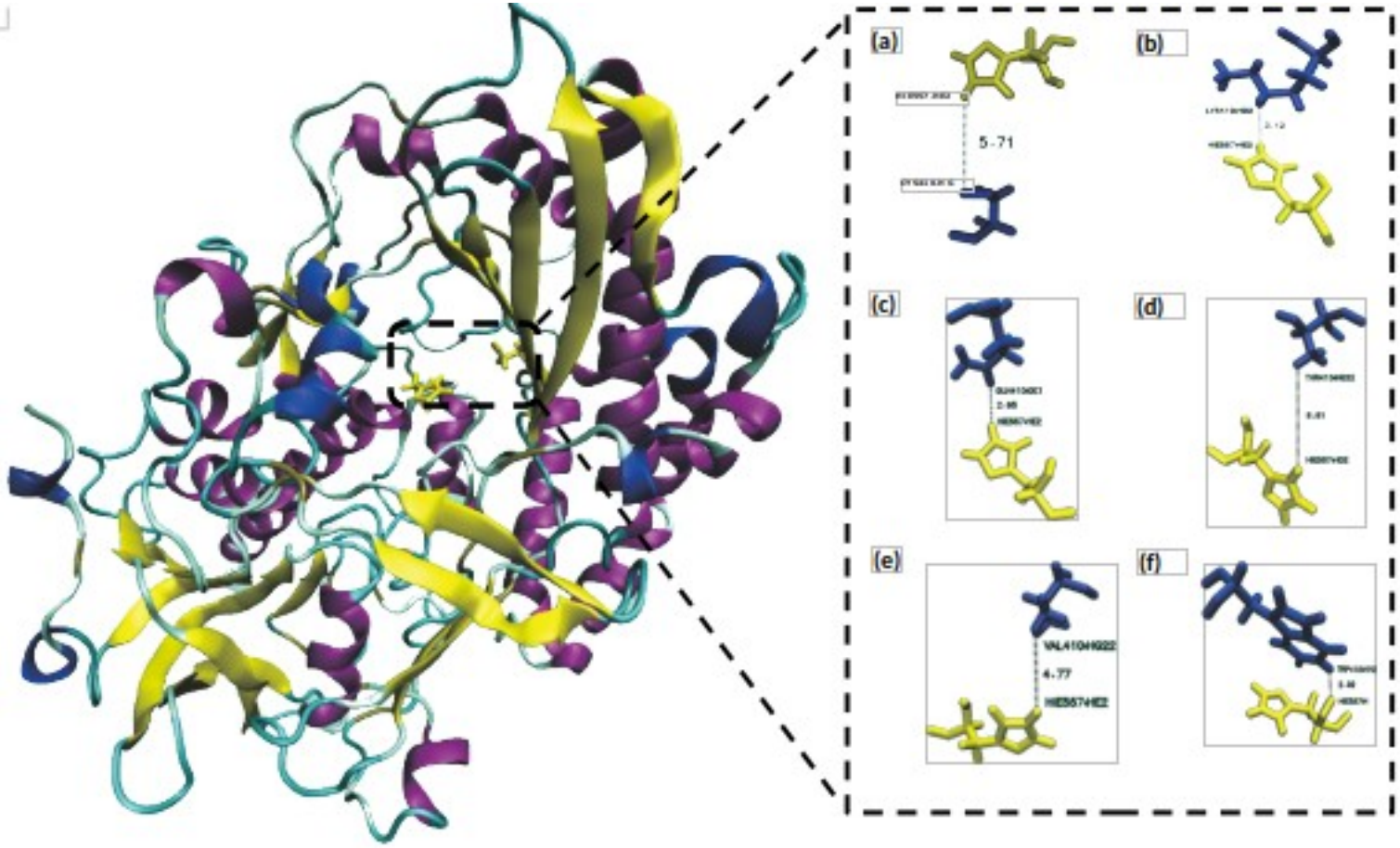


**Figure 7:** Visualization of the interaction between E412 and H559 mutant residues in the mutant structures (a) E412C, (b) E412K, (c) E412Q, (d) E412T, (e) E412V, (f) E412W.

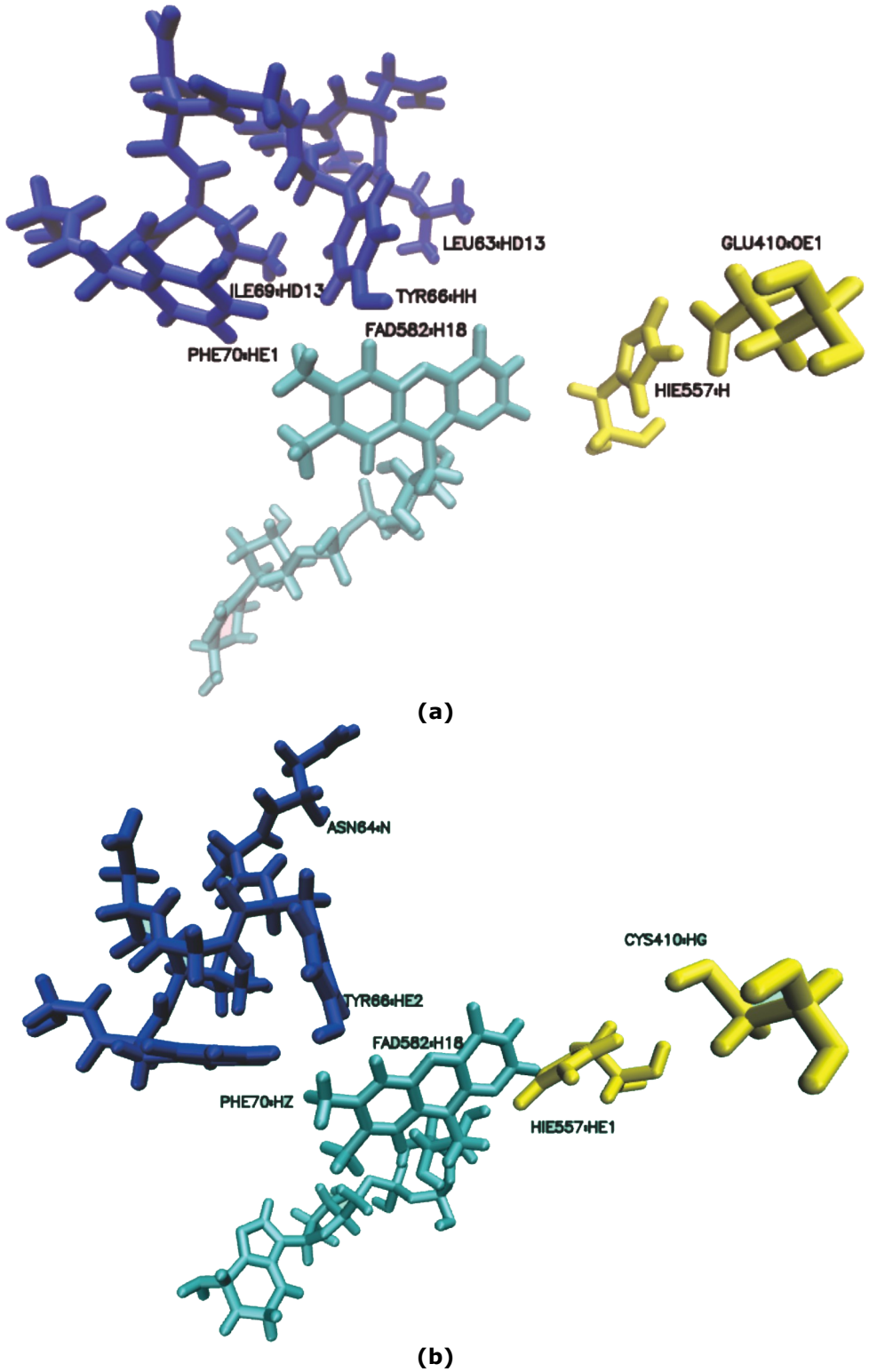


**Figure 8:** Visualization of the interaction distance between H559-m412 residues and 3-10 helix motif residues. (a) wild-type (b) E412C (c) E412K (d) E412Q (e) E412T (f) E412V (g) E412W.

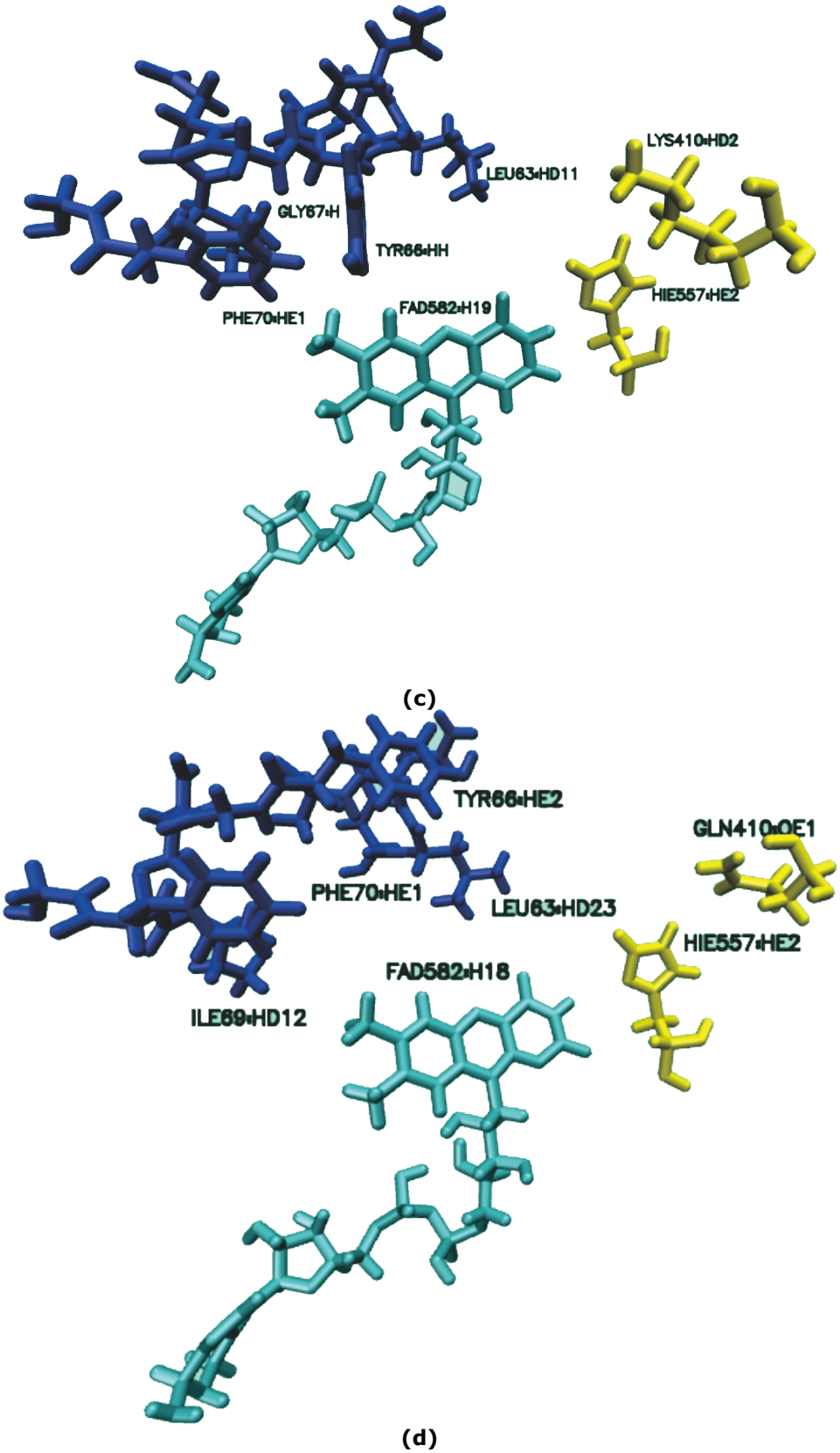


**Figure 8 (contd.):** Visualization of the interaction distance between H559-m412 residues and 3-10 helix motif residues. (a) wild-type (b) E412C (c) E412K (d) E412Q (e) E412T (f) E412V (g) E412W.

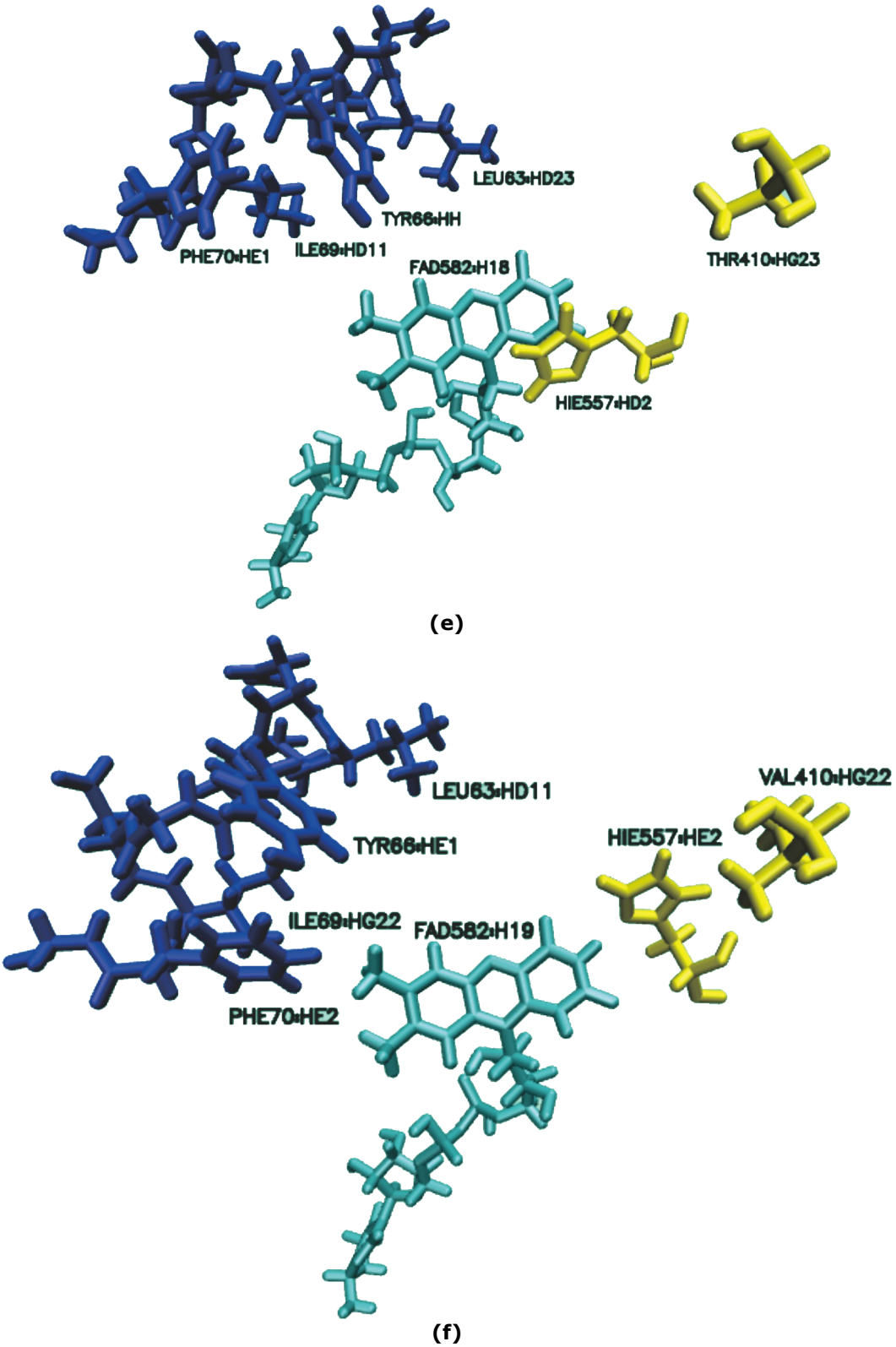


**Figure 8 (contd.):** Visualization of the interaction distance between H559-m412 residues and 3-10 helix motif residues. (a) wild-type (b) E412C (c) E412K (d) E412Q (e) E412T (f) E412V (g) E412W.

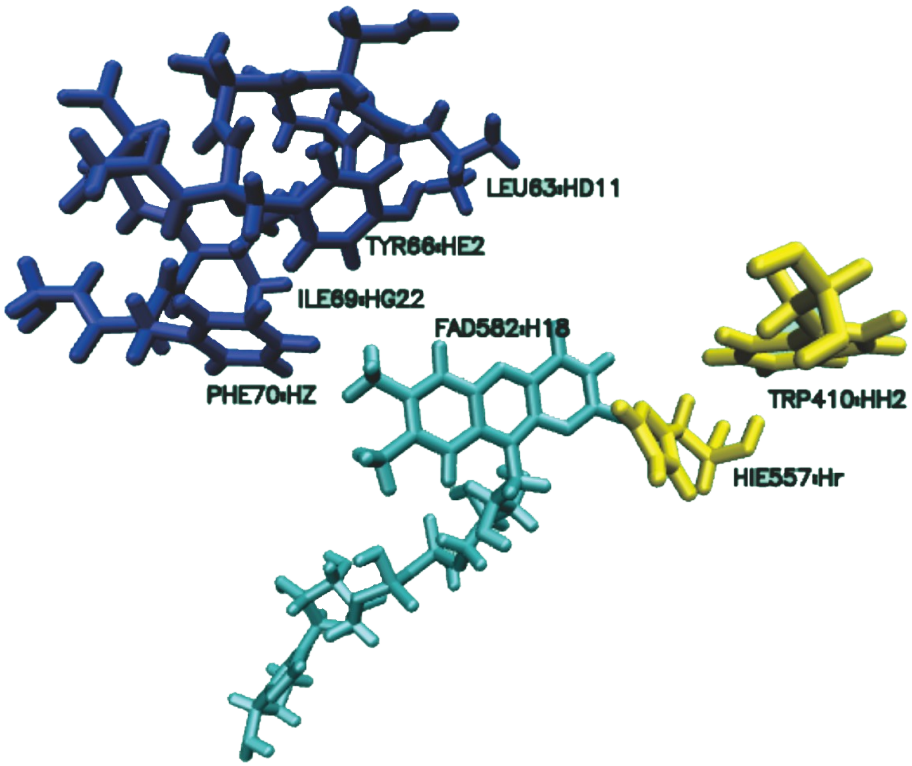


**(g)**

**Figure 8 (contd.):** Visualization of the interaction distance between H559-m412 residues and 3-10 helix motif residues. (a) wild-type (b) E412C (c) E412K (d) E412Q (e) E412T (f) E412V (g) E412W.

**GOx-IPBCC Mutant Structure Stability Based on Salt Bridge**

The stability of the GOx-IPBCC mutant structure was further evaluated using salt bridge analysis that emerged during a simulation time of 50 ns. As a probability from molecular dynamics simulations, the salt bridge bond interactions are formed by chance (30). The analysis results show approximately 45 pairs of salt bridges formed during the simulation time and 21 pairs of salt bridges that always appear in each mutant structure (Table 3). The probability of the emergence of salt bridge interactions plays a vital role in the thermal stability of proteins (31).

Several pairs of salt bridges appear to be broken or not maintained by the mutant structure, including the E372-R398 salt bridge pairs (Table 3); the salt bridge pair D317-K304 failed to maintain by the E412Q and E412T mutants. Maulana et al., (2019) revealed that the GOx-IPBCC structure has thermal stability, which is influenced by the formation of salt bridges.

**Table 3:** Comparison of the results of the analysis of the salt bridge pairs that emerged in the 50 ns simulation of the mutant structure of the GOx-IPBCC enzyme.

| Wild-type | E412C | E412K | E412Q | E412T | E412V | E412W |
|---|---|---|---|---|---|---|
| D19-K280 | D19-K280 | D19-K280 | D19-K280 | D19-K280 | D19-K280 | D19-K280 |
| E38-R237 | E38-R237 | E38-R237 | E38-R237 | E38-R237 | E38-R237 | E38-R237 |
| D55-R228 | D55-R228 | D55-R228 | D55-R228 | D55-R228 | - | D55-R228 |
| E61-R228 | E61-R228 | E61-R228 | E61-R228 | E61-R228 | E61-R228 | E61-R228 |
| D75-R93 | D75-R93 | D75-R93 | D75-R93 | D75-R93 | D75-R93 | D75-R93 |
| D132-K114 | D132-K114 | D132-K114 | D132-K114 | D132-K114 | D132-K114 | D132-K114 |
| E142-R111 | E142-R111 | E142-R111 | E142-R111 | E142-R111 | E142-R111 | E142-R111 |
| D175-K150 | D175-K150 | D175-K150 | D175-K150 | D175-K150 | D175-K150 | D175-K150 |
| D179-K150 | D179-K150 | D179-K150 | D179-K150 | D179-K150 | D179-K150 | D179-K150 |
| E219-R145 | E219-R145 | E219-R145 | E219-R145 | E219-R145 | E219-R145 | E219-R145 |
| E266-K250 | E266-K250 | E266-K250 | E266-K250 | E266-K250 | E266-K250 | E266-K250 |
| E282-R543 | E282-R543 | E282-R543 | E282-R543 | E282-R543 | E282-R543 | E282-R543 |

| Wild-type | E412C | E412K | E412Q | E412T | E412V | E412W |
|---|---|---|---|---|---|---|
| D317-K524 | D317-K524 | D317-K304 | - | D317-K304 | D317-K304 | D317-K524 |
| D317-K304 | D317-K304 | D317-K524 | - | - | D317-K524 | D317-K304 |
| E372-R398 | - | - | - | - | - | E372-R398 |
| D422-R510 | D422-R510 | D422-R510 | - | A422-R510 | A422-R510 | D422-R510 |
| D440-K271 | D440-K271 | D440-K271 | D440-K271 | D440-K271 | D440-K271 | D440-K271 |
| E456-K370 | E456-K370 | E456-K370 | E456-K370 | E456-K370 | E456-K370 | E456-K370 |
| D571-R35 | D571-R35 | D571-R35 | D571-R35 | D571-R35 | D571-R35 | D571-R35 |
| D576-R535 | D576-R535 | D576-R535 | D576-R543 | D576-R535 | D576-R535 | D576-R535 |
| D576-R543 | D576-R543 | D576-R543 | D576-R535 | D576-R543 | D576-R543 | D576-R543 |

The stability of the GOx-IPBCC mutant structure based on RMSD data describes fairly good stability during the simulation time. However, the RMSF and secondary structure data revealed that the GOx-IPBCC structure was unstable at the residue region 61-73, namely, the conformation of the 3-10 helix structure changed. Especially in the mutant structure E412K, E412Q, E412V and E412W, which undergo structural conformational changes during the simulation time.

**MMPBSA Calculation and Hydrogen Bond Interaction**

Hydrogen bonding interactions between β-D-glucose and GOx-IPBCC enzymes were also analyzed to obtain information about the effect of mutations on the substrate-binding site (Table 4). Based on the analysis results, the dynamics of changes in substrate binding by the GOx-IPBCC mutant structure did not change significantly. Residues that appear on the results of the analysis of the wild-type structure can still be found in the mutant structure; in the mutant structure, the hydrogen bonding interactions of the other residues even increased, especially in the E412K and E412T mutants. On the other hand, in the E412C, E412Q, E412V and E412W mutant structures, the number of residues interacting with hydrogen bonds was reduced. The E412 residue is a catalytic residue that stabilizes the H559 catalytic residue to bind the substrate. Thus, some of the mutations in this study affect the substrate binding-pose, especially on hydrogen interactions.

Based on the results of molecular dynamics simulations, the ligand complex and structure of the GOx-IPBCC mutant analyzed using the MMPBSA simulation method. This method is the final method widely used to validate molecular docking data by calculating the value of free energy ($\Delta G$) (32,33). The free energy of ligand binding by proteins is measured by calculating the entropic contribution during the reaction. Another approach to estimating binding affinity is calculating the free energy along the path connecting the two thermodynamic states: the ligand in its bound and unbound state (34).

The MMPBSA simulation was run using the Amber 18. The results revealed that the free energy data of ligand binding during the molecular dynamics simulation time showed that the mutant structures E412C, E412K, E412Q, E412T, and E412V. Has higher free energy values ($\Delta G$) compared to the wild type structures (20.63 kcal/mol) or has a weaker free energy value because the more negative the binding energy of the ligand, and there is one mutant structure that has a negative free energy value or better, that is -22.79 in the E412W mutant. These results indicate that the analyzed mutant structure largely reduces the interaction or ligand binding free energy by the GOx-IPBCC enzyme.

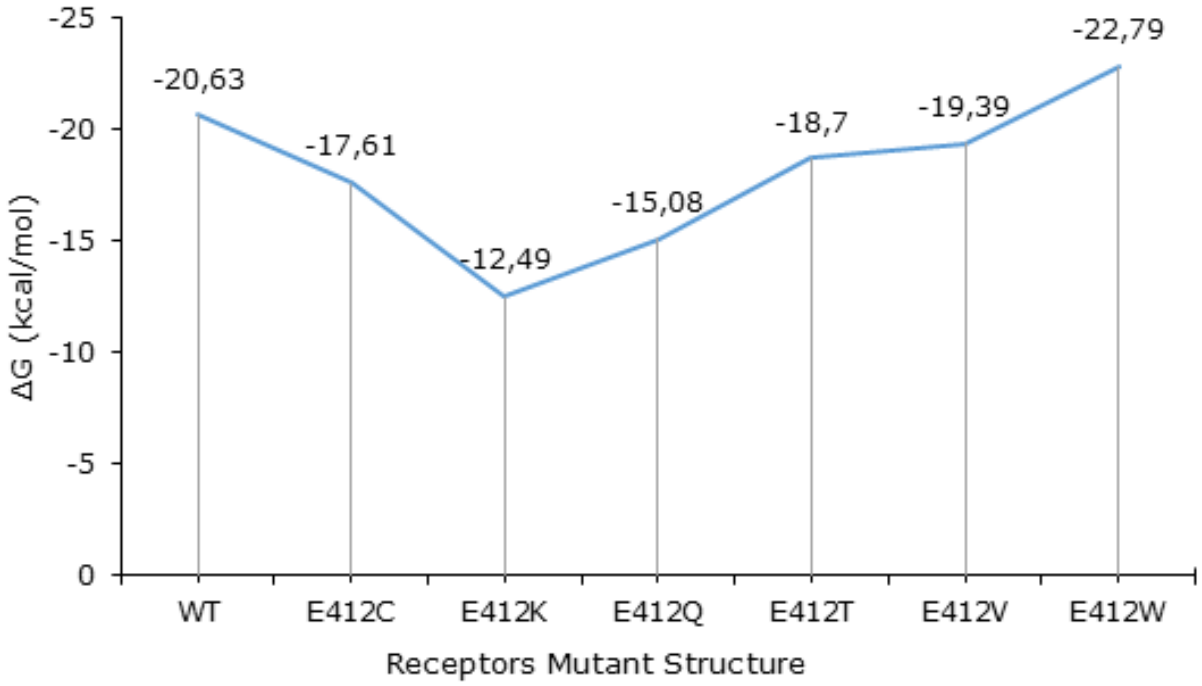


**Figure 9:** Comparative profile of free energy value (*ΔG*) of β-D-glucose ligand binding by GOx-IPBCC mutant structure.

The bond interaction profile formed during the simulation time of 50 ns between the mutant structure and the β-D-glucose ligand gave quite different results. There is a loss of interacting catalytic residues. The loss of this interaction is predicted that the enzyme structure loses its catalytic ability. The mutants that experienced a loss of interaction of H516 and H5559 catalytic residues were E412K and E412V mutants, while the E412C and E412T mutants lost one interaction of H516 catalytic residues, and the E412W mutant did not lose interaction with the two catalytic residues.

**Table 4:** Residual data that interacts hydrogen bonding with the substrate (β-D-glucose) during the molecular dynamics simulation time of 50 ns.

| Receptor | Hydrogen Bond | Payload Mutant |
|---|---|---|
| *Wild-type* | Tyr66, Thr108, Gln327, Thr329, Arg510, Asn512, His514, His557, FAD | Polar |
| E412C | Tyr66, Thr108, Asp422, Arg510, Asn512, His557, FAD | Polar |
| E412K | Tyr66, Asp68, Gly107, Thr108, Thr329, Ile336, Asp414, Ala416, Ser420, Asp422, Arg510, Asn512, FAD | Positive |
| E412Q | Tyr66, Thr108, Asp422, Arg510, Asn512, His514, His557, FAD | Polar |
| E412T | Tyr66, Thr108, Thr329, Asp422, Arg510, Pro511, Asn512, His557, FAD | Polar |
| E412V | Tyr66, Val104, Gly106, Asp422, Arg510, Asn512, FAD | Nonpolar |
| E412W | Thr108, Arg510, Asn512, His514, His557 | Nonpolar |

## CONCLUSION

The results showed that the catalytic mutation of residue E412 in the GOx-IPBCC enzyme significantly affected the structural stability and binding of the GOx-IPBCC enzyme to the ligand. These results were confirmed by the molecular dynamics analysis method, which showed that the structure of the mutant increased and decreased in the binding energy value, in the E412W mutant,

which decreased, and the E412C, E412K, E412Q, E412T, and E412V mutants increased. In addition, based on RMSF and salt bridge data, it is known that the structure of the E412C, E412T and E412W mutants are the mutants that have the best structural stability. These results are expected to add information about increasing the utilization of GOx-IPBCC enzymes, especially those that require enzyme activity with higher ΔG values, such as EFC (enzymatic fuel cell) for E412C and E412T mutant types, or to improve molecular quality-holding energy, namely E412W.

## CONFLICT OF INTEREST

There is no conflict to declare.

## REFERENCES


1. Obut S, Bahar T. Glucose oxidase immobilized biofuel cell flow channel geometry analysis by CFD simulations. Turkish J Chem. 2019;43(5):1486–502. Available from: <URL>.

2. Sumaiya A, Trivedi R. A Review on Glucose OxidaseDepartment of Microbiology. Shree Ramkrishna Institute of Applied Sciences. int J curr Microbiol App sci. 2015;4:636–40.

3. Kriaa M, Kammoun R. Producing Aspergillus tubingensis CTM507 Glucose oxidase by Solid state fermentation versus submerged fermentation: Process optimization and enzyme stability by an intermediary metabolite in relation with diauxic growth. J Chem Technol Biotechnol. 2016;91(5):1540–50. Available from: <URL>.

4. Anas A, Gunny N. Studies on the production of Glucose oxidase by Aspergillus terreus UniMAP AA-1. Universiti Malaysia Perlis (UniMAP); 2011.

5. Gutierrez A, Wallraf A, Balaceanu A, Bocola M, Davari M, Meier T, et al. How to engineer glucose oxidase for mediated electron transfer. Biotechnol Bioeng. 2018;115(10):2405–15. Available from: <URL>.

6. Subiyono S, Martsiningsih MA, Gabrela D. Gambaran Kadar Glukosa Darah Metode GOD-PAP (Glucose Oxsidase–Peroxidase Aminoantypirin) Sampel Serum dan Plasma EDTA (Ethylen Diamin Terta Acetat). J Teknol Lab. 2016;5(1):45–8.

7. Ostafe R, Fontaine N, Frank D, Ng Fuk Chong M, Prodanovic R, Pandjaitan R, et al. One-shot optimization of multiple enzyme parameters: Tailoring glucose oxidase for pH and electron mediators. Biotechnol Bioeng. 2020;117(1):17–29. Available from: <URL>.

8. Mano N. Engineering glucose oxidase for bioelectrochemical applications. Bioelectrochemistry [Internet]. 2019;128:218–40. Available from: <URL>.

9. Leech D, Kavanagh P, Schuhmann W. Enzymatic fuel cells: Recent progress. Electrochim Acta [Internet]. 2012;84:223–34. Available from: <URL>.

10. Vogt S, Schneider M, Schäfer-Eberwein H, Nöll G. Determination of the pH dependent redox potential of glucose oxidase by spectroelectrochemistry. Anal Chem. 2014;86(15):7530–5. Available from: <URL>.

11. Triana R. Pemurnian dan karakterisasi enzim glukosa oksidase dari isolat lokal Aspergillus niger (IPBCC.08610). Institut Pertanian Bogor; 2013.

12. Indriani A. Pemurnian dengan kromatografi penukar anion dan karakterisasi glukosa oksidase dari aspergillus niger IPBCC 08.610. Institut Pertanian Bogor; 2018.

13. Maulana FA, Ambarsari L, Wahyudi ST. Homology modeling and structural dynamics of the glucose oxidase. Indones J Chem. 2019;20(1):43–53.

14. Kurniatin PA, Ambarsari L, Khanza ADA, Setyawati I, Seno DSH, Nurcholis W. Characteristics of glucose oxidase gene (GGOx) from Aspergillus niger IPBCC 08.610. J Kim Val. 2020;6(1):10–9.

15. Dwiastuti R, Radifar M, Marchaban M, Noegrohati S, Istyastono E., Dwiastuti R, et al. Molecular Dynamics Simulations and Empirical Observations on Soy Lecithin Liposome Preparation. Indones J Chem. 2016;16(2):222–8.

16. Sharma P, Joshi T, Mathpal S, Joshi T, Pundir H, Chandra S, et al. Identification of natural inhibitors against Mpro of SARS-CoV-2 by molecular docking, molecular dynamics simulation, and MM/PBSA methods. J Biomol Struct Dyn [Internet]. 2020;0(0):1–12. Available from: Available from: <URL>.

17. Petrović D, Frank D, Kamerlin S, Hoffmann K, Strodel B. Shuffling active site substate populations affects catalytic activity: The case of glucose oxidase. ACS Catal. 2017;7(9):6188–6197. Available from: <URL>.

18. Mu Q, Cui Y, Tian Y, Hu M, Tao Y, Wu B. Thermostability improvement of the glucose oxidase from Aspergilus niger for efficient gluconic acid production via computational design. Biol Macromol. 2019;136:1060–8. Available from: <URL>.

19. Tu T, Wang Y, Huang H, Wang Y, Jiang X, Wang Z, et al. Improving the thermostability and catalytic efficiency of glucose oxidase from Aspergillus niger by molecular evolution. Food Chem. 2019;281:163–70. Available from: <URL>.

20. Kaczmarski JA, Mahawaththa MC, Feintuch A, Clifton BE, Adams LA, Goldfarb D, et al. Altered conformational sampling along an evolutionary trajectory changes the catalytic activity of an enzyme. Nat Commun [Internet]. 2020;11(1):1–14. Available from: <URL>.

21. Case I, Ben-Shalom S, Brozell D, Cerutti T, Cheatham I, Cruzeiro T, et al. AMBER 2018. San Francisco: University of California; 2018.

22. Myers J, Grothaus G, Narayanan S, Onufriev A. A simple clustering algorithm can be accurate enough for use in calculations of pKs in macromolecules. Proteins Struct Funct Bioinforma. 2006;63(4):928–38. Available from: <URL>.

23. Anandakrishnan R, Aguilar B, Onufriev A V. H++ 3.0: Automating pK prediction and the preparation of biomolecular structures for atomistic molecular modeling

and simulations. Nucleic Acids Res. 2012;40(W1):W537–41. Available from: <URL>.

24. Miller BR, McGee TD, Swails JM, Homeyer N, Gohlke H, Roitberg AE. MMPBSA.py: An efficient program for end-state free energy calculations. J Chem Theory Comput. 2012;8(9):3314–21. Available from: <URL>.

25. Wohlfahrt G, Witt S, Hendle J, Schomburg D, Kalisz H, Hecht H. 1.8 and 1.9 Å resolution structures of the Penicillium amagasakiense and Aspergillus niger glucose oxidases as a basis for modelling substrate complexes. Acta Crystallogr Sect D Biol Crystallogr. 1999;969–77. Available from: <URL>.

26. Singh R, Tiwari M, Singh R, Lee J. From protein engineering to immobilization: promising strategies for the upgrade of industrial enzymes. Int J Mol Sci. 2013; (14):1232–77. Available from: <URL>.

27. Guterres H, Im W. Improving protein-ligand docking results with high-throughput molecular dynamics simulations. J Chem Inf Model. 2020;60(4):2189–98. Available from: <URL>.

28. Yu H, Yan Y, Zhang C, Dalby PA. Two strategies to engineer flexible loops for improved enzyme thermostability. Sci Rep. 2017;7(1):1–15. Available from: <URL>.

29. Vieira P, Simão R, Morais C, Henrique J. $3_{10}$ Helices in channels and other membrane proteins. J Gen Physiol. 2010;136(6):585–92. Available from: <URL>.

30. Basu S, Biswas P. Salt-bridge dynamics in intrinsically disordered proteins: A trade-off between electrostatic interactions and structural flexibility. Biochim Biophys Acta - Proteins Proteomics [Internet]. 2018;1866(5–6):624–41. Available from: <URL>.

31. Chen L, Li X, Wang R, Fang F, Yang W, Kan W. Thermal stability and unfolding pathways of hyperthermophilic and mesophilic periplasmic binding proteins studied by molecular dynamics simulation. J Biomol Struct Dyn. 2016;34(7):1576–89. Available from: <URL>.

32. Anuar NFSK, Wahab RA, Huyop F, Amran SI, Hamid AAA, Halim KBA, et al. Molecular docking and molecular dynamics simulations of a mutant Acinetobacter haemolyticus alkaline-stable lipase against tributyrin. J Biomol Struct Dyn. 2020;1–13. Available from: <URL>.

33. Ji B, Liu S, He X, Man VH, Xie XQ, Wang J. Prediction of the binding affinities and selectivity for CB1 and CB2 ligands using homology modeling, molecular docking, molecular dynamics simulations, and MM-PBSA binding free energy calculations. ACS Chem Neurosci. 2020;11(8):1139–58. Available from: <URL>.

34. Aldeghi M, Bodkin MJ, Knapp S, Biggin PC. Statistical analysis on the performance of molecular mechanics poisson-boltzmann surface area versus absolute binding free energy calculations: bromodomains as a case study. J Chem Inf Model. 2017;57(9):2203–21. Available from: <URL>.